THE JOURNAL OF BIOLOGICAL CHEMISTRY VOL. 285, NO. 50, pp. 39544–39550, December 10, 2010

Metabolic Flux Analysis of the Mixotrophic Metabolisms in the Green Sulfur Bacterium *Chlorobaculum tepidum*[*] [S]

Received for publication, July 9, 2010, and in revised form, September 5, 2010 Published, JBC Papers in Press, October 11, 2010, DOI 10.1074/jbc.M110.162958

Xueyang Feng[‡1], **Kuo-Hsiang Tang**[§1], **Robert E. Blankenship**[§¶], **and Yinjie J. Tang**[‡2]

From the Departments of [‡]*Energy, Environmental and Chemical Engineering,* [§]*Biology, and* [¶]*Chemistry, Washington University, St. Louis, Missouri 63130*

The photosynthetic green sulfur bacterium *Chlorobaculum tepidum* assimilates CO_2 and organic carbon sources (acetate or pyruvate) during mixotrophic growth conditions through a unique carbon and energy metabolism. Using a ^{13}C-labeling approach, this study examined biosynthetic pathways and flux distributions in the central metabolism of *C. tepidum*. The isotopomer patterns of proteinogenic amino acids revealed an alternate pathway for isoleucine synthesis (via citramalate synthase, CimA, CT0612). A ^{13}C-assisted flux analysis indicated that carbons in biomass were mostly derived from CO_2 fixation via three key routes: the reductive tricarboxylic acid (RTCA) cycle, the pyruvate synthesis pathway via pyruvate: ferredoxin oxidoreductase, and the CO_2-anaplerotic pathway via phosphoenolpyruvate carboxylase. During mixotrophic growth with acetate or pyruvate as carbon sources, acetyl-CoA was mainly produced from acetate (via acetyl-CoA synthetase) or citrate (via ATP citrate lyase). Pyruvate:ferredoxin oxidoreductase converted acetyl-CoA and CO_2 to pyruvate, and this growth-rate control reaction is driven by reduced ferredoxin generated during phototrophic growth. Most reactions in the RTCA cycle were reversible. The relative fluxes through the RTCA cycle were 80∼100 units for mixotrophic cultures grown on acetate and 200∼230 units for cultures grown on pyruvate. Under the same light conditions, the flux results suggested a trade-off between energy-demanding CO_2 fixation and biomass growth rate; *C. tepidum* fixed more CO_2 and had a higher biomass yield ($Y_{X/S}$, mole carbon in biomass/mole substrate) in pyruvate culture ($Y_{X/S} = 9.2$) than in acetate culture ($Y_{X/S} = 6.4$), but the biomass growth rate was slower in pyruvate culture than in acetate culture.

Chlorobaculum tepidum is a representative green sulfur bacterium that is ecologically significant in global cycling of carbon, nitrogen, and sulfur (1, 2). The *C. tepidum* genome has been sequenced, and the genetic tools for creating *C. tepidum* mutant strains have been developed to make transposon-based mutations or targeted gene disruptions, which offer great potential to engineer *C. tepidum* for future applications (3). The annotated genome reveals unique aspects in carbon and energy metabolism in *C. tepidum*. Instead of using the Calvin-Benson cycle for CO_2 assimilation as in most photosynthetic organisms, *C. tepidum* captures energy from light and uses it along with electrons, primarily derived from oxidation of sulfur compounds, to drive the reductive tricarboxylic acid cycle (RTCA)[3] for synthesis of building block molecules (3). *C. tepidum* can grow mixotrophically with acetate or pyruvate as the organic carbon source (2). Although recent research has been performed on the carbon and energy metabolism of *C. tepidum* (4, 5), rigorous quantification of the metabolic pathway activities has not yet been achieved. To provide quantitative readout of the metabolic functions and regulatory mechanisms, this study has performed ^{13}C-assisted metabolic flux analysis of *C. tepidum* in the following steps: 1) growing cultures of *C. tepidum* with ^{13}C-labeled acetate or pyruvate, 2) using gas chromatography (GC)-MS to measure the resulting labeling pattern in key metabolites, and 3) deciphering *in vivo* metabolisms via a flux model (6). Isotopic labeling and metabolic flux analysis have been developed to identify the active biosynthesis pathways (7–10) and measure the global enzymatic reaction rates (11, 12). The cell-wide quantification of intracellular metabolism can bridge the gap between genome annotations and final metabolic outputs and has been applied for characterizing numerous environmental microorganisms, including *Escherichia coli* (13, 14), *Saccharomyces cerevisiae* (15, 16), *Bacillus subtilis* (17), *Geobacter metallireducens* (18), *Shewanella oneidensis* (19), and *Synechocystis* sp. (20)., etc. This paper reports on the first studies of the fluxomics of mixotrophic metabolism in the green sulfur bacteria and provides complementary information to previous genomic and proteomic studies.

EXPERIMENTAL PROCEDURES

^{13}C-labeled Experiments—C. tepidum cultures were grown anaerobically at temperatures ranging from 46–50 °C in low intensity light (100 ± 10 micromoles/m^2/s). The medium composition (1 liter) was $Na_2EDTA\text{-}2H_2O$ (0.015 g), $MgSO_4\text{-}7H_2O$ (0.22 g), $CaCl_2\text{-}2H_2O$ (0.08 g), NaCl (0.45 g), NH_4Cl (0.45 g), $Na_2S_2O_3\text{-}5H_2O$ (2.6 g), KH_2PO_4 (0.57 g), MOPS buffer (2.4 g), trace element stock (1.2 ml), vitamin B_{12} stock (0.08 mg), $NaHCO_3$ (2.3 g), and $Na_2S\text{-}9H_2O$ (0.8 g). All chemicals were purchased from Sigma-Aldrich. The carbon source for the trace experiments was [1-^{13}C]acetate (purity > 98%,

* This work was supported in part by National Science Foundation Career Grant MCB0954016 (to Y. J. T.). This work was also supported by Grant NNX08AP62G from the Exobiology program of NASA (to R. E. B.).

[S] The on-line version of this article (available at http://www.jbc.org) contains supplemental Tables S1–S4 and Fig. S1.

[1] Both authors contributed equally to this article.

[2] To whom correspondence should be addressed. Tel.: 314-935-3441; Fax: 314-935-7211; E-mail: yinjie.tang@seas.wustl.edu.

[3] The abbreviations used are: RTCA, the reductive tricarboxylic acid; DCW, dry cell weight; MOPS, 4-morpholinepropanesulfonic acid.

0.83 g/liter) or [2-^{13}C] acetate (purity > 98%, 0.83 g/liter) for cultures growing on acetate, or [3-^{13}C]pyruvate (purity > 98%, 1.1 g/liter) for cultures growing on pyruvate. The ^{13}C-labeled acetate and pyruvate were purchased from Cambridge Isotope Laboratories. Cell growth was monitored at A_{625}. 1% cultures (100-fold dilution) in the exponential growth phase were used to inoculate fresh media with ^{13}C-labeled substrates. To reduce the effect of nonlabeled carbon from the initial stock, cells were subcultured twice in the same labeled medium. Biomass was sampled at two time points (4-h interval) in the middle exponential growth phase, and the labeling patterns of proteinogenic amino acids in the biomass were measured. The invariability of amino acid labeling during the two time points confirmed the pseudo-steady-state metabolism in tracer experiments.

Metabolites and Isotopomer Analysis—The amount of pyruvate and acetate during the growth period was determined by enzymatic assays (21–23). For GC-MS measurement of amino acid labeling, the biomass was harvested by centrifugation and hydrolyzed using 6 M HCl (24 h at 100 °C) (19, 24). The amino acids were derivatized in 0.2 ml of tetrahydrofuran and 0.2 ml of *N*-(tert-butyl dimethylsilyl)-*N*-methyl-trifluoroacetamide (Sigma-Aldrich). A gas chromatograph (Hewlett-Packard model 7890A; Agilent Technologies) equipped with a DB5-MS column (J&W Scientific, Folsom, CA) and a mass spectrometer (model 5975C; Agilent Technologies) were used for analyzing metabolite labeling profiles. Four types of charged fragments were detected by GC-MS for all of the amino acids (see Table 1 and Fig. 1); the $[M-57]^+$ or $[M-15]^+$ group (containing unfragmented amino acids); and the $[M-159]^+$ or $[M-85]^+$ group (containing amino acids that had lost an α-carboxyl group). For each type of fragments, the labeling patterns were represented by M_0, M_1, M_2, etc, which were fractions of unlabeled, singly labeled, and doubly labeled amino acids. The effects of natural isotopes on isotopomer labeling patterns were corrected by previously reported algorithms (25). To compare the relative contributions of carbon substrates and CO_2 to mixotrophic biomass synthesis, the substrate utilization ratio R was calculated based on the labeling patterns of unfragmented amino acid *X* (*e.g.* alanine) (7),

$$\frac{0.98 \times n \times V_{sub} + 0.01 \times V_{CO_2}}{m \times V_{sub} + V_{CO_2}} = \frac{(\sum_{i=1}^{C} i \times M_i)}{C} \quad \text{(Eq. 1)}$$

$$R = \frac{m V_{sub}}{V_{CO_2}} \quad \text{(Eq. 2)}$$

where R ratio reflects the carbon flux ratio of labeled carbon substrate to unlabeled CO_2 for producing the corresponding amino acid *X* (mol carbon from substrate/mol carbon from CO_2); $M_i$is the GC-MS isotopomer fraction for a given amino acid. *C* is the total number of carbon atoms in the amino acid molecule. V_{sub} is the uptake of ^{13}C-labeled organic substrates, V_{CO2} is the uptake of CO_2; 0.98 is the purity of the labeled carbon substrate, 0.01 is the natural abundance of ^{13}C, *m* is the total number of carbons in the substrate molecule, and *n* is the total number of labeled carbons in the substrate molecule.

Metabolic Flux Analysis—The pathway map of *C. tepidum* was generated based on genome annotation from the KEGG database (Kyoto Encyclopedia of Genes and Genomes) and transcription analysis of several key pathways (26). The simplified pathway map includes the reductive tricarboxylic acid cycle, CO_2-anaplerotic pathway, gluconeogenesis pathway, and pentose phosphate pathway (supplemental Fig. S1 and Table S1). The development of a pseudo-steady-state flux model has been discussed before (19, 27, 28). In brief, the substrate (acetate or pyruvate) uptake rate was measured and normalized to 100 units. The biomass production was determined based on our previous paper (26). The biomass composition for macromolecules such as protein and fatty acids was assigned based on that of *E. coli* (13). The fluxes to biomass pools were loosely constrained by the estimated dry cell weight (DCW) and biomass compositions. These fluxes were used as initial inputs to the isotopomer model and optimized by isotopomer labeling information (Table 1 and supplemental Table S2). The remaining unknown intracellular fluxes were determined by reaction stoichiometry and atom/isotopomer mapping matrices in an iterative scheme (supplemental Table S3). The reaction reversibility was calculated using the exchange coefficient (18),

$$v_i^{exch} = \frac{exch_i}{1 - exch_i} \quad \text{(Eq. 3)}$$

where v_i^{exch} is the exchange flux defined as the smaller of the forward and backward fluxes, and $exch_i$ is the exchange coefficient with the range of 0–1. (If the reaction is irreversible, $exch_i$ is 0; if the reaction is "freely" reversible, $exch_i$ is close to 1.) The flux combinations were searched to minimize of the objective function (19),

$$\epsilon(v_n) = \sum_{i=1}^{a} \left(\frac{M_i - N_i(v_n)}{\delta_i} \right)^2 \quad \text{(Eq. 4)}$$

where v_n are the unknown fluxes to be optimized in the program, M_i is the measured MS data, N_i is the corresponding model-simulated MS data, and δ_i is the corresponding S.D. in GC-MS data (1~2%). The unknown metabolic fluxes were searched to minimize ϵ. The model was solved by IPOPT (Interior Point Optimizer), which is a software package for large-scale nonlinear optimization. To avoid getting trapped in a local optimal minimum, multiple initial guesses (>100) were used for model calculation to obtain the global solution.

To estimate the confidence interval for the calculated fluxes, a Monte Carlo approach was employed (14). In brief, the isotopomer concentration data sets were generated by adding 2% of normally distributed measurement noise to actual measured isotopomer data. The same optimization routine was used to estimate flux distribution from these data sets. Confidence limits for each flux value were obtained from the probability distribution of calculated fluxes resulting from the simulated data sets ($n = 100$). To determine the requirements of cellular metabolism for energy

TABLE 1

Isotopic labeling patterns in amino acids from *Chlorobaculum tepidum*

The S.D. for GC-MS measurement were based on the duplicate experiments (n = 2), with an S.D. below 2%.

Carbon source	Amino acids	Fragments	M_0	M_1	M_2
[1-^{13}C]Acetate	Ala	$[M-57]^+$	0.45	0.54	0.01
		$[M-159]^+$	0.44	0.53	0.03
	Gly	$[M-57]^+$	0.54	0.46	0.00
		$[M-85]^+$	0.54	0.46	
	Ser	$[M-57]^+$	0.46	0.52	0.02
		$[M-159]^+$	0.47	0.53	0.00
	Leu	$[M-159]^+$	0.21	0.43	0.33
	Ile	$[M-159]^+$	0.21	0.43	0.33
	Asp	$[M-57]^+$	0.64	0.35	0.01
		$[M-159]^+$	0.65	0.34	0.01
	Glu	$[M-57]^+$	0.63	0.33	0.04
		$[M-159]^+$	0.63	0.33	0.04
	Phe	$[M-57]^+$	0.11	0.29	0.36
		$[M-159]^+$	0.12	0.30	0.36
[2-^{13}C]Acetate	Ala	$[M-57]^+$	0.43	0.56	0.01
		$[M-159]^+$	0.42	0.54	0.04
	Gly	$[M-57]^+$	0.94	0.06	0.00
		$[M-85]^+$	0.95	0.05	
	Ser	$[M-57]^+$	0.44	0.55	0.01
		$[M-159]^+$	0.45	0.55	0.00
	Leu	$[M-159]^+$	0.13	0.25	0.36
	Ile	$[M-159]^+$	0.14	0.25	0.36
	Asp	$[M-57]^+$	0.61	0.38	0.00
		$[M-159]^+$	0.62	0.37	0.00
	Glu	$[M-57]^+$	0.62	0.35	0.03
		$[M-159]^+$	0.63	0.34	0.03
	Phe	$[M-57]^+$	0.13	0.26	0.36
		$[M-159]^+$	0.14	0.26	0.35
	His	$[M-57]^+$	0.16	0.35	0.36
		$[M-159]^+$	0.28	0.48	0.22
[3-^{13}C]Pyruvate	Ala	$[M-57]^+$	0.67	0.32	0.01
		$[M-159]^+$	0.65	0.30	0.05
	Gly	$[M-57]^+$	0.96	0.04	0.00
		$[M-85]^+$	0.97	0.03	
	Ser	$[M-57]^+$	0.71	0.28	0.01
		$[M-159]^+$	0.71	0.28	0.01
	Leu	$[M-159]^+$	0.47	0.38	0.12
	Ile	$[M-159]^+$	0.47	0.39	0.12
	Asp	$[M-57]^+$	0.82	0.17	0.00
		$[M-159]^+$	0.83	0.15	0.01
	Glu	$[M-57]^+$	0.75	0.20	0.05
		$[M-159]^+$	0.76	0.20	0.04
	Phe	$[M-57]^+$	0.38	0.41	0.17
		$[M-159]^+$	0.38	0.40	0.18
	His	$[M-57]^+$	0.46	0.41	0.11
		$[M-159]^+$	0.56	0.34	0.08

and reducing power, the relative consumption rates of ATP, NADH, NADPH, and ferredoxin were quantified based on the flux distributions in the central metabolic pathways and biomass synthesis rates.

Calculation of Biomass Yield—The biomass yield (mol of carbon in biomass/mol of substrate) was calculated based on the substrate uptake rates (mol of substrate/liter/h) and biomass growth rates (g DCW/liter/h). The molecular formula for *C. tepidum* was assumed to be $CH_{1.8}O_{0.5}N_{0.2}P_{0.02}$ (molecular weight (MW) ≈ 25.5) (29). The biomass yield was calculated by (yield = biomass growth rate (g/liter/h)/molecular weight of biomass (g/mol))/substrate uptake rate (mol/liter/h).

RESULTS AND DISCUSSION

Carbon Utilization during Mixotrophic Growth—During exponential growth with pyruvate and acetate, *C. tepidum* had the growth rates of 0.12 h^{-1} and 0.17 h^{-1}, respectively. In the trace experiments, the labeled carbons were detected in all amino acids (Table 1), suggesting utilization of acetate or pyruvate to synthesize all building blocks. Table 2 shows the ratio of carbon utilization (organic carbon *versus* CO_2) for mixotrophic synthesis of proteinogenic amino acids. For acetate culture, the substrate utilization ratio for Ala (precursor, pyruvate) was 0.60, which indicated that carbons in pyruvate were mainly derived from labeled acetate. Pyruvate is the precursor for both the gluconeogenesis pathway and the pentose phosphate pathway, so the R ratios (Equation 1) of Ser and Phe are similar to that of alanine. The substrate utilization ratio of His was high (0.96) for culture with [2-^{13}C]acetate because the His precursor C1 pool (N^5,N^{10}-methylene-tetrahydrofolate) was highly labeled. This carbon was derived from acetate by following route [2-^{13}C]acetate → [3-^{13}C]pyruvate → [3-^{13}C]Ser → [^{13}C]C1 pool.

TABLE 2

Carbon substrate utilization ratios in amino acids from *Chlorobaculum tepidum*

The carbon source utilization ratio (organic substrate/CO_2 fixation) for amino acid synthesis was calculated according to Equation 1.

Amino acids	Carbon sources		
	[1-^{13}C]acetate + $NaHCO_3$	[2-^{13}C]acetate + $NaHCO_3$	[3-^{13}C]pyruvate + $NaHCO_3$
Ala	0.60	0.60	0.48
Ser	0.58	0.58	0.42
Asp	0.20	0.22	0.12
Glu	0.18	0.18	0.21
His	NA[a]	0.96	0.38
Phe	0.62	0.64	0.26

[a] Isotopomer labeling pattern for histidine was not detected under [1-^{13}C]acetate + $NaHCO_3$ due to the weak signal to noise ratio in GC-MS.

In the mixotrophic culture with acetate, the R ratios for aspartate and glutamate (~0.2) were significantly lower than the other amino acids. Aspartate and glutamate were synthesized from the RTCA cycle, so the small R values indicated that the unlabeled CO_2 was the dominant carbon source for synthesizing metabolites in the RTCA cycle. In pyruvate culture, the substrate utilization ratios of amino acids (Ala, Phe, Ser, and Asp) were all lower than in acetate culture, indicating a higher contribution of CO_2 to synthesize building blocks.

Analysis of Amino Acid Biosynthesis Pathways—Growing in a completely defined medium, *C. tepidum* was able to synthesize all amino acids from CO_2 and organic carbon sources using the annotated pathways. Interestingly, the labeling patterns of Leu and Ile from tracer experiments were found to be identical, which indicated that the two amino acids shared the same precursors. Ile is commonly synthesized via threonine ammonia-lyase, with Thr and pyruvate as the precursors, whereas Leu is synthesized from pyruvate and acetyl-CoA. In the [2-^{13}C]acetate trace experiment, both Thr and pyruvate are singly labeled, which could lead only to doubly labeled Ile, instead of the triply labeled Ile detected by GC-MS. Such an observation is consistent with the fact that a gene encoding threonine ammonia-lyase has not been annotated in the genome of *C. tepidum*. On the other hand, an alternative pathway for Ile biosynthesis (*i.e.* threonine-independent pathway) has been recently identified in several bacteria (8, 9, 24, 30), where Ile is synthesized from acetyl-CoA and pyruvate (*i.e.*

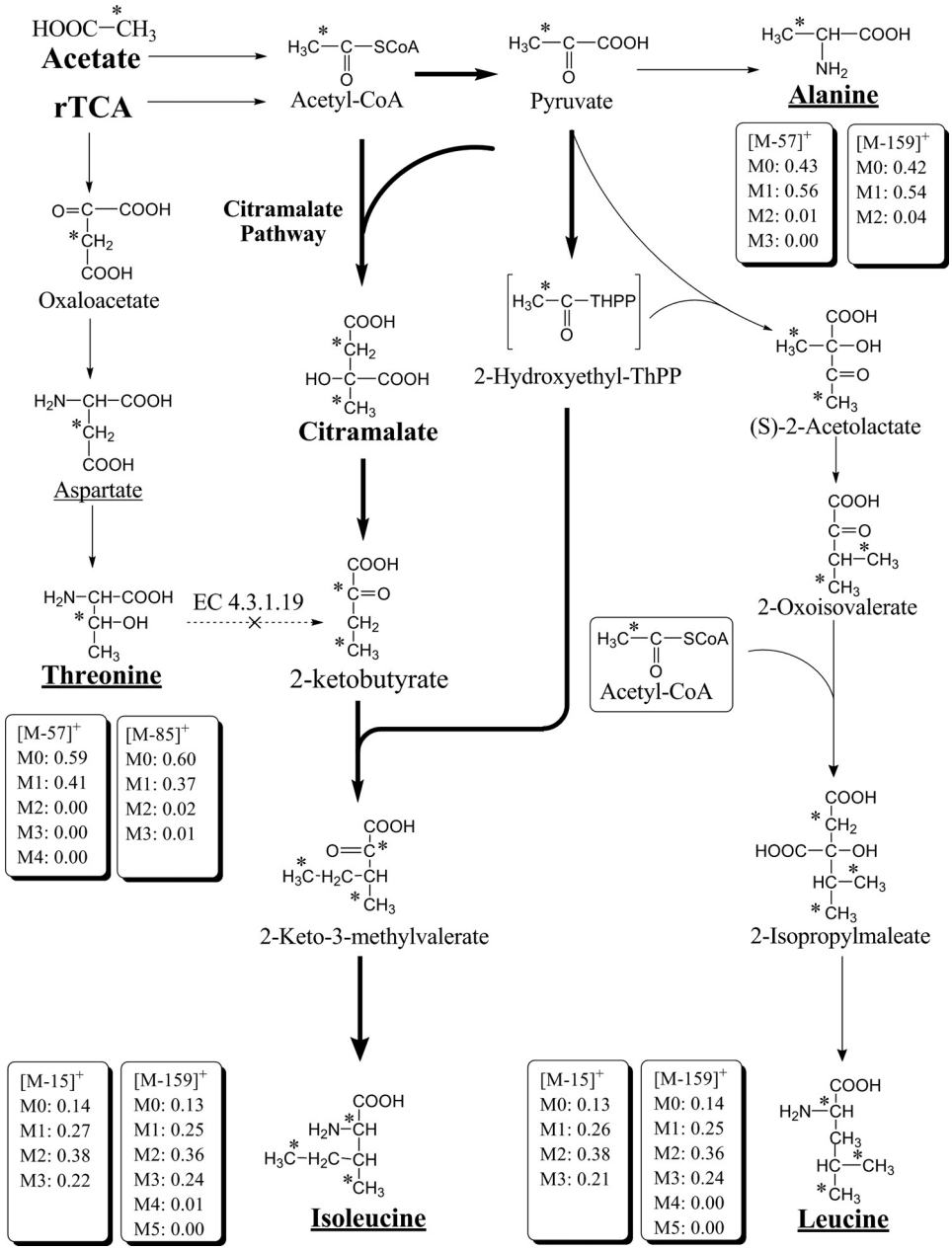

FIGURE 1. **Citramalate pathway for isoleucine biosynthesis in *C. tepidum* (using [2-^{13}C]acetate and $NaHCO_3$ as carbon sources).** The *asterisks* indicate the positions of labeled carbon. The *dashed lines* indicate inactive pathways.

using the same precursors as Leu) through the formation of citramalate as the intermediate (Fig. 1). A search in the genome of *C. tepidum* for the gene for citramalate synthase (*CimA*) as found in *Geobacter* (9) returned a high identity for CT0612 (~52%), supporting the presence of the citramalate pathway for Ile synthesis.

Central Carbon Metabolic Pathways—The genome annotation from the KEGG database indicates that 1) pyruvate:ferredoxin oxidoreductase (*porA*, CT1628) converts pyruvate to acetyl-CoA (an end product from RTCA cycle); 2) phosphoenolpyruvate is derived from pyruvate via pyruvate phosphate dikinase (CT1682), and 3) phosphoenolpyruvate is fed into the TCA cycle via the CO_2-anaplerotic pathway (Fig. 2). The fraction of nonlabeled Asp (M_0 = 0.64, Table 1) was much higher than that of Ala (M_0 = 0.45, Table 1) in trace experiments with [1-^{13}C]acetate, which indicated that nonlabeled oxaloacetate was also generated through CO_2 fixation via the RTCA cycle. Furthermore, similar labeling patterns of Ala (precursor, pyruvate) and Ser (precursor, glycerate-3-P) confirmed that the carbon flux through the gluconeogenesis pathway was mainly from pyruvate.

The flux analysis results are shown in Fig. 2. In general, predicted labeling patterns of all amino acids were good matches with the measured isotopomer data (Fig. 3). Under acetate growth conditions, acetyl-CoA could be generated from acetate uptake or as the end product through the RTCA cycle. Fluxes through pyruvate:ferredoxin oxidoreductase, the RTCA cycle, and the CO_2-anaplerotic pathway were ~152, 80–100, and ~30 units, respectively (Fig. 2). Meanwhile, the flux ratio of the gluconeogenesis pathway to the RTCA cycle

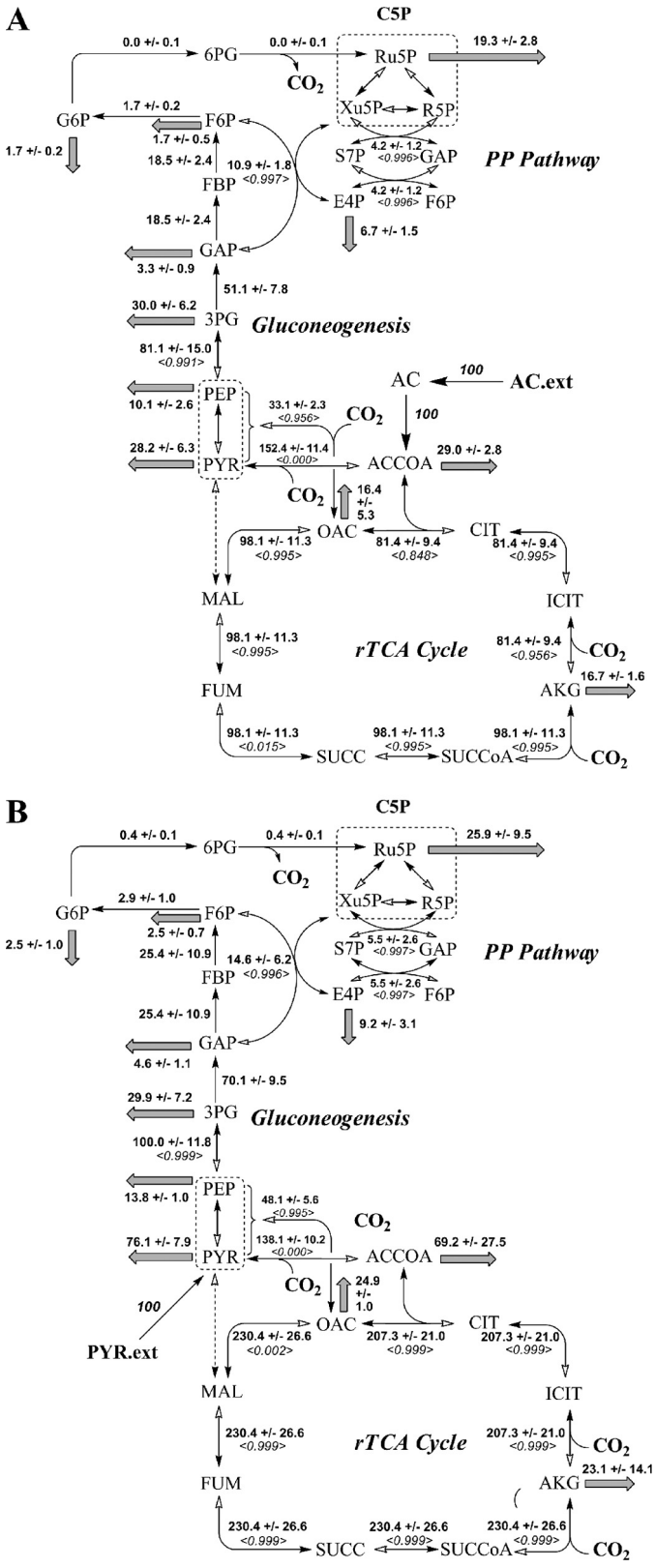

FIGURE 2. **Metabolic flux distribution in *C. tepidum*.** *A*, net flux distribution in acetate growth conditions (based on [2-^{13}C]acetate culture). *B*, net flux distribution in pyruvate growth conditions. The S.D. and exchange coefficients are marked by flux ± S.D. and < exchange coefficient >, respectively. The inactive pathways are marked with *dashed lines*. The calculated biomass yield (moles of carbon in biomass/mol of substrate): pyruvate culture ($Y_{X/S}$ = 9.2); acetate culture ($Y_{X/S}$ = 6.4). *S7P*, sedoheptulose-7-phosphate; *SUCC*, succinate; *SUCCoA*, succinyl-CoA; *Xu5P*, xylulose-5-phosphate; *3PG*, 3-phosphoglycerate; *6PG*, 6-phosphogluconate; *AC*, intracellular acetate; *ACCOA*, acetyl-coenzyme A; *AC.ext*, extracellular acetate; *AKG*, α-ketoglutarate; *CIT*, citrate; *E4P*, erythrose-4-phosphate; *F6P*, fructose-6-phosphate; *FBP*, fructose 1,6-bisphosphate; *FNR*, ferredoxin-NAD(P)$^+$ reductase; *FUM*, fumarate; *G6P*, glucose-6-phosphate; *GAP*, glyceraldehyde 3-phosphate; *ICIT*, isocitrate; *MAL*, malate; *OAC*, oxaloacetate; *PEP*, phosphoenolpyruvate; *PYR*, intracellular pyruvate; *PYR.ext*, extracellular pyruvate; *R5P*, ribose-5-phosphate; *Ru5P*, ribulose-5-phosphate; *PP*, pentose phosphate.

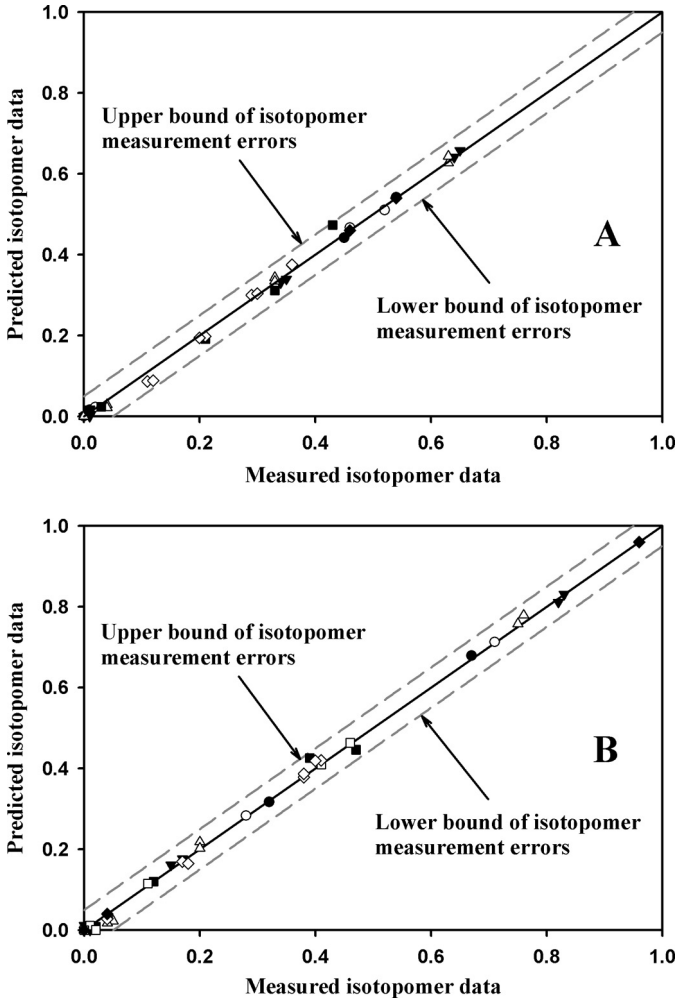

FIGURE 3. **Model quality test for acetate metabolism (*A*) and pyruvate metabolism (*B*).** ●, alanine; ○, serine; ▼, aspartate, Δ, glutamate; ■, leucine; □, histidine; ◇, phenylalanine; and ◆, glycine.

was close to 1:1. The oxidative pentose phosphate pathway (glucose-6-phosphate → 6-phosphogluconate → ribulose-5-phosphate) was inactive under our experimental conditions. Compared with mixotrophic growth with acetate, the flux distribution during pyruvate growth demonstrated different patterns. In general, the fluxes into the RTCA cycle and CO_2-anaplerotic pathway were much higher (200–230 units and ~50 units, respectively), and thus, more CO_2 was fixed. The flux ratio of the gluconeogenesis pathway to the RTCA cycle was reduced to 1:2, whereas acetyl-CoA was generated only from the RTCA cycle. The oxidative pentose phosphate pathway was not active (flux < 1 unit) under pyruvate mixotrophic growth (or acetate mixotrophic growth).

In the mixotrophic cultures grown on acetate or pyruvate, most reactions in the RTCA cycle were freely reversible (with

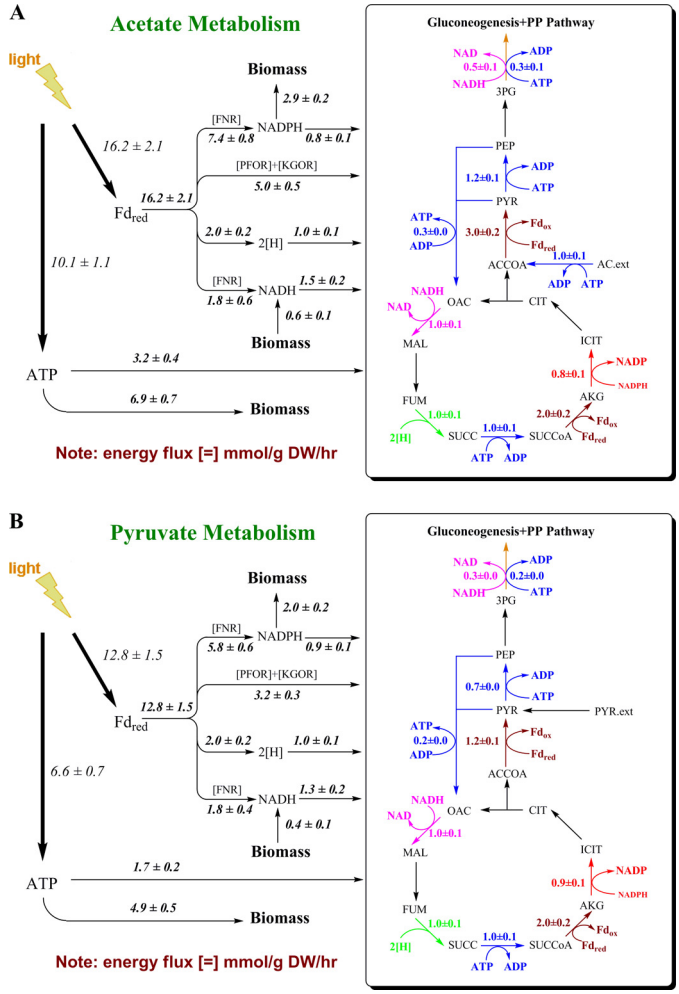

FIGURE 4. **Proposed energy metabolism in *C. tepidum*.** *A*, energy requirement (mmol/g DCW/h) in acetate growth conditions. *B*, energy requirement (mmol/g DCW/h) in pyruvate growth conditions. The intracellular energy metabolism was quantified in the framed figures based on the relative flux distributions. (Detailed calculations can be found in supplemental Table S4, *A* and *B*). *Arrows* pointing to the framed figure indicated the energy demand of intracellular metabolism. *Arrows* pointing to biomass indicate the energy demand of biomass accumulation. *Arrows* pointing from light indicated the entire energy harvested by *C. tepidum*. The light reaction produces reduced ferredoxin and ATP. NADPH and NADH are mainly generated by ferredoxin-NAD(P)$^+$ reductase. Biomass (protein) synthesis can also generate a small amount of NADH, as indicated in the figure. *SUCC*, succinate; *SUCCoA*, succinyl-CoA; *3PG*, 3-phosphoglycerate; *ACCOA*, acetyl-coenzyme A; *AC.ext*, extracellular acetate; *AKG*, α-ketoglutarate; *CIT*, citrate; *FNR*, ferredoxin-NAD(P)$^+$ reductase; *FUM*, fumarate; *ICIT*, isocitrate; *MAL*, malate; *OAC*, oxaloacetate; *PEP*, phosphoenolpyruvate; *PYR*, intracellular pyruvate; *KGOR*, 2-ketoglutarate ferredoxin oxidoreductase; Fd_{red}, reduced ferredoxin; Fd_{ox}, oxidized ferredoxin; *PP*, pentose phosphate.

an exchange coefficient close to 1). The reversibility is consistent with the physiological free energy changes in the RTCA cycle, where the standard Gibbs free energy for most reactions of the TCA cycle is positive so that the magnitude of the reaction equilibrium constants is small (31). Furthermore, pyruvate:ferredoxin oxidoreductase catalyzes a reversible reaction between pyruvate and acetyl-CoA (pyruvate + CoA + $2Fd_{ox} \leftrightarrow$ acetyl-CoA + CO_2 + $2Fd_{red}$ + $2H^+$). (Fd_{red} indicates reduced ferredoxin, and Fd_{ox} indicates oxidized ferredoxin.) However, metabolic flux analysis of the mixotrophic metabolism indicates that the net flux of this enzymatic reaction was from acetyl-CoA to pyruvate (32). The direction of the pyruvate:ferredoxin oxidoreductase pathway indicates that the reduced ferredoxin from phototrophic processes made the reaction for pyruvate synthesis thermodynamically favorable.

Energy Metabolism of C. tepidum—The mixotrophic metabolism of *C. tepidum* consumes energy harvested from light. Because the oxidative pentose phosphate pathway and normal TCA cycle are not fully functional, the energy (NADPH and NADH) generation mainly depends on the light reactions. Based on the metabolic flux distribution and previous measurement of the absolute uptake rates of carbon substrates and biomass growth (26), the light energy harvested for central metabolism and biomass growth was approximately quantified (Fig. 4). In general, the photons absorbed by pigments (*e.g.* bacteriochlorophylls) initiate the electron flow and oxidize sulfide. The electrons are used to reduce ferredoxin and generate NAD(P)H (2, 3). Concomitant with the oxidation of the reduced ferredoxin, the essential cofactors for energy metabolism (*i.e.* NADPH and NADH) are mainly generated by ferredoxin-NAD(P)$^+$ reductase (2, 33). Meanwhile, the oxidation of sulfide also creates a proton motive force for ATP production. The generated ATP, cofactors, and reduced ferredoxin then become the "driver" for the mixotrophic metabolism and the RTCA cycle for energy-demanding CO_2 fixation. Fig. 4 shows that the ATP, NADH, and NADPH fluxes into biomass and the RTCA cycle are stronger in acetate-grown cultures than in pyruvate-grown cultures, supporting a higher growth rate during mixotrophic growth with acetate. On the other hand, the calculated biomass yield (mol of carbon in biomass/mol of substrate) was higher for pyruvate culture ($Y_{X/S}$ = 9.2) than for acetate ($Y_{X/S}$ = 6.4), based on our previous experiments (26), which is consistent with the fact that the normalized fluxes through RTCA are higher in pyruvate culture than acetate culture. Accordingly, pyruvate metabolism has more CO_2 fixation (but slower growth rate).

Acknowledgment—We thank Professor Yixin Chen (Computer Science and Engineering Department, Washington University) for helping with model optimization.

REFERENCES

1. Wahlund, T. M., Woese, C. R., Castenholz, R. W., and Madigan, M. T. (1991) *Arch. Microbiol.* **156,** 81–90
2. Frigaard, N. U., Chew, A. G., Li, H., Maresca, J. A., and Bryant, D. A. (2003) *Photosynth. Res.* **78,** 93–117
3. Eisen, J. A., Nelson, K. E., Paulsen, I. T., Heidelberg, J. F., Wu, M., Dodson, R. J., Deboy, R., Gwinn, M. L., Nelson, W. C., Haft, D. H., Hickey, E. K., Peterson, J. D., Durkin, A. S., Kolonay, J. L., Yang, F., Holt, I., Umayam, L. A., Mason, T., Brenner, M., Shea, T. P., Parksey, D., Nierman, W. C., Feldblyum, T. V., Hansen, C. L., Craven, M. B., Radune, D., Vamathevan, J., Khouri, H., White, O., Gruber, T. M., Ketchum, K. A., Venter, J. C., Tettelin, H., Bryant, D. A., and Fraser, C. M. (2002) *Proc. Natl. Acad. Sci. U.S.A.* **99,** 9509–9514
4. Wahlund, T. M., and Tabita, F. R. (1997) *J. Bacteriol.* **179,** 4859–4867
5. Charnock, C., Refseth, U. H., and Sirevåg, R. (1992) *J Bacteriol.* **174,** 1307–1313
6. Tang, Y. J., Martin, H. G., Myers, S., Rodriguez, S., Baidoo, E. E., and Keasling, J. D. (2009) *Mass. Spectrom. Rev.* **28,** 362–375
7. Feng, X., Banerjee, A., Berla, B., Page, L., Wu, B., Pakrasi, H. B., and Tang, Y. J. (2010) *Microbiology* **156,** 2566–2574

8. Wu, B., Zhang, B., Feng, X., Rubens, J. R., Huang, R., Hicks, L. M., Pakrasi, H. B., and Tang, Y. J. (2010) *Microbiology* **156,** 596–602
9. Risso, C., Van Dien, S. J., Orloff, A., Lovley, D. R., and Coppi, M. V. (2008) *J. Bacteriol.* **190,** 2266–2274
10. Pingitore, F., Tang, Y., Kruppa, G. H., and Keasling, J. D. (2007) *Analytical Chemistry* **79,** 2483–2490
11. Tang, Y. J., Meadows, A. L., Kirby, J., and Keasling, J. D. (2007) *Journal of Bacteriology* **189,** 894–901
12. Tang, Y. J., Martin, H. G., Dehal, P. S., Deutschbauer, A., Llora, X., Meadows, A., Arkin, A., and Keasling, J. D. (2009) *Biotechnol. Bioeng.* **102,** 1161–1169
13. Fischer, E., Zamboni, N., and Sauer, U. (2004) *Anal. Biochem.* **325,** 308–316
14. Zhao, J., and Shimizu, K. (2003) *J. Biotechnol.* **101,** 101–117
15. Kleijn, R. J., Geertman, J. M., Nfor, B. K., Ras, C., Schipper, D., Pronk, J. T., Heijnen, J. J., van Maris, A. J., and van Winden, W. A. (2007) *FEMS Yeast Res.* **7,** 216–231
16. Sonderegger, M., Jeppsson, M., Hahn-Hägerdal, B., and Sauer, U. (2004) *Appl. Environ. Microbiol.* **70,** 2307–2317
17. Fischer, E., and Sauer, U. (2005) *Nat. Genet.* **37,** 636–640
18. Tang, Y. J., Chakraborty, R., Martín, H. G., Chu, J., Hazen, T. C., and Keasling, J. D. (2007) *Appl. Environ. Microbiol.* **73,** 3859–3864
19. Tang, Y. J., Hwang, J. S., Wemmer, D. E., and Keasling, J. D. (2007) *Appl. Environ. Microbiol.* **73,** 718–729
20. Yang, C., Hua, Q., and Shimizu, K. (2002) *Metab. Eng.* **4,** 202–216
21. Tang, K. H., Feng, X., Tang, Y. J., and Blankenship, R. E. (2009) *PLoS One* **4,** e7233
22. Howell, B. F., McCune, S., and Schaffer, R. (1979) *Clin. Chem.* **25,** 269–272
23. Tang, K. H., Yue, H., and Blankenship, R. E. (2010) *BMC Microbiol.* **10,** 150
24. Feng, X., Mouttaki, H., Lin, L., Huang, R., Wu, B., Hemme, C. L., He, Z., Zhang, B., Hicks, L. M., Xu, J., Zhou, J., and Tang, Y. J. (2009) *Appl. Environ. Microbiol.* **75,** 5001–5008
25. Wahl, S. A., Dauner, M., and Wiechert, W. (2004) *Biotechnol. Bioeng.* **85,** 259–268
26. Tang, K. H., and Blankenship, R. E. (July 22, 2010) *J. Biol. Chem.* **285,** 35848–35854
27. Sauer, U., Lasko, D. R., Fiaux, J., Hochuli, M., Glaser, R., Szyperski, T., Wüthrich, K., and Bailey, J. E. (1999) *J. Bacteriol.* **181,** 6679–6688
28. Tang, Y. J., Sapra, R., Joyner, D., Hazen, T. C., Myers, S., Reichmuth, D., Blanch, H., and Keasling, J. D. (2009) *Biotechnol Bioeng.* **102,** 1377–1386
29. Stephanopoulos, G. N., Aristidou, A. A., and Nielsen, J. (1998) *Metabolic Engineering Principles and Methodologies*, 1st Ed., pp. 119–126, Academic Press, San Diego, CA
30. Tang, Y., Pingitore, F., Mukhopadhyay, A., Phan, R., Hazen, T. C., and Keasling, J. D. (2007) *J. Bacteriol.* **189,** 940–949
31. Voet, D., Voet, J. G., and Pratt, C. W. (2008) *Fundamentals of Biochemistry*, 3rd Ed., pp. 586, John Wiley & Sons, Inc., Hoboken, New Jersey
32. Furdui, C., and Ragsdale, S. W. (2000) *J. Biol. Chem.* **275,** 28494–28499
33. Seo, D., and Sakurai, H. (2002) *Biochim. Biophys. Acta.* **1597,** 123–132